X-ray phase contrast imaging: Transmission functions separable in cylindrical coordinates

Guohua Cao,[1,a)] Theron Hamilton,[1] Christopher M. Laperle,[2] Christoph Rose-Petruck,[1] and Gerald J. Diebold[1,b)]
[1]*Department of Chemistry, Brown University, Providence, Rhode Island 02912, USA*
[2]*The Liver Research Center, Rhode Island Hospital and Warren Alpert Medical School, Brown University, Providence, Rhode Island 02912, USA*

(Received 30 November 2007; accepted 14 October 2008; published online 19 May 2009)

A Fresnel–Kirchhoff integral can be used to calculate x-ray phase contrast images when the transmission function is known. Here expressions for image intensity are derived for objects with axial symmetry for an x-ray source with non-vanishing dimensions. An expression for the image intensity is given for an x-ray source whose intensity distribution is described by a Gaussian function, from which an expression for the limiting case of a point source of radiation is found. The expressions for image intensity are evaluated for cases where the magnification is substantially greater than one, as would be employed in biological imaging. Experiments using a microfocus x-ray tube and charge coupled device camera are reported to determine the capability of the method for imaging small spherical objects, such as gold particles, which might find application as contrast agents in biomedical imaging. © *2009 American Institute of Physics*. [DOI: 10.1063/1.3112129]

I. INTRODUCTION

The appeal of the x-ray in-line phase contrast method[1,2] for soft tissue imaging lies in its strong contrast for rapid variations in density, which appear in the image as bright and dark outlines at the perimeters of objects. The in-line method is sensitive to absorption so that the image contains features both from absorption contrast, as in a conventional x-ray shadowgraph and phase contrast as well. If absorption contrast is not of primary interest since the method relies on the deflection of x-radiation rather than their absorption, it is possible to employ hard, weakly absorbed x-radiation providing a significantly lower absorbed radiation dose than that in conventional x-ray shadowgraphy. In order to produce phase contrast in an image, the x-ray source must have a high degree of spatial coherence; hence, x-ray synchrotrons[3–5] or microfocus x-ray tubes[6–8] are typically used as radiation sources. A further feature of employment of sources with high spatial coherence, in addition to the benefit of phase contrast in the image, is that if the image recording device is chosen to have high resolution, the obvious advantage of high spatial resolution also becomes characteristic of the method adding to its overall utility as an imaging diagnostic.

From a knowledge of the transmission function $q(X,Y)$, where X and Y are the coordinates on the object perpendicular to the propagation direction of the radiation,[8] the image produced with the in-line method can be determined from a Fresnel–Kirchhoff integral.[9,10] Here, we derive a expressions for in-line phase contrast imaging using a Fresnel–Kirchhoff integral for objects with cylindrical symmetry referred to the propagation direction of the x-radiation, that is, where the phase function for the object to be imaged can be expressed as a function of a radial coordinate R only. The derivation in Sec. II gives the electric field for a source with an arbitrary intensity distribution. Section III gives an expression for the image plane intensity for a Gaussian source intensity distribution. Section IV gives limiting expressions for the image intensity for a point source and for the limiting case of a large source-to-object distance. Experiments carried out with the goal of determining the capability of phase contrast imaging for detecting spherical objects are reported in Sec. V. The work presented here focuses on imaging where the magnification of the object and the resolution are appropriate for detection of small density variations in biological specimens.

II. ELECTRIC FIELD AT THE IMAGE PLANE

The electric field f at the image plane for an x-ray source of unit electric field amplitude is governed by the Fresnel–Kirchhoff integral[11] over a plane Σ_0,

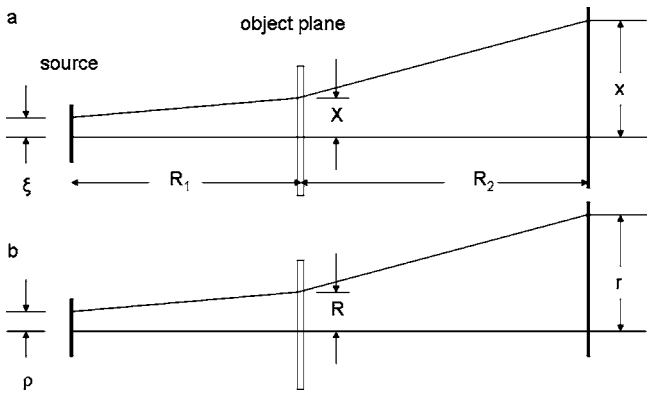

FIG. 1. Schematic drawing of the coordinates used in the evaluation of the Fresnel–Kirchhoff integral for phase contrast imaging with a nonvanishing, circularly symmetric source. The object and source are taken as lying on a line along the normal to the image plane. In (a) the Cartesian coordinates on the source, object, and image planes are denoted as (ξ,η), (X,Y), and (x,y), respectively. In (b) the radial coordinates are denoted as (ρ,θ), (R,Φ), and (r,ϕ), respectively.

a)Electronic mail: gcao@physics.unc.edu.
b)Electronic mail: gerald_diebold@brown.edu.

$$f(r) = \frac{i}{\lambda}\int_{\Sigma_0} \frac{e^{-ik|\mathbf{r}-\mathbf{r}'|}}{|\mathbf{r}-\mathbf{r}'|} d\sigma, \tag{1}$$

where, as shown in Fig. 1, $\mathbf{r}$ is the coordinate in the image plane, $\mathbf{r}'$ is the coordinate on the object plane, k is the wave number of the radiation, and $d\sigma$ is an area element in the plane. For a point source or radiation located on the source plane at $\mathbf{r}''$, the electric field in the object plane is of the form $e^{-ik|\mathbf{r}''-\mathbf{r}'|}/|\mathbf{r}''-\mathbf{r}'|$. If D is the distance between planes, both $|\mathbf{r}-\mathbf{r}'|$ and $|\mathbf{r}''-\mathbf{r}'|$ are of the form $|\mathbf{r}_a-\mathbf{r}_b| = \sqrt{D^2+(x_a-x_b)^2+(y_a-y_b)^2}$, which can be expanded to first order in Cartesian coordinates to give the usual Fresnel approximation[8] to Eq. (1). Consider an object with a transmission function q. When f is then expressed in cylindrical coordinates defined as

$$\xi = \rho\cos\theta \quad X = R\cos\Phi \quad x = r\cos\varphi,$$

$$\eta = \rho\sin\theta \quad Y = R\sin\Phi \quad y = r\sin\varphi,$$

the electric field becomes

$$f(r) = \frac{i}{\lambda R_1 R_2} e^{-ik(R_1+R_2)} \int_0^\infty \int_0^{2\pi} e^{-(ik/2R_1)[\rho^2+R^2-2\rho R\cos(\theta-\Phi)]-(ik/2R_2)[r^2+R^2-2rR\cos(\varphi-\Phi)]} q(R) R dR d\Phi, \tag{2}$$

where $q(R)$ is the transmission function for an object whose phase and absorption are a function of the coordinate R alone. The transmission function, which describes the phase deviation ϕ and the (intensity) absorption μ on traversal through the object, can be taken to be of the form

$$q(R) = \begin{cases} e^{i\phi(R)-\mu(R)/2} & \text{for } R \le R_0 \\ 1 & \text{for } R > R_0, \end{cases} \tag{3}$$

where R_0 is the radius of the object. Owing to the symmetry of both the object and source, the integrand in Eq. (2) must be independent of φ and can be evaluated at $\varphi=0$.

The integral over R in Eq. (2) can be written as a sum of two integrals of the form

$$f(r) = \int_0^\infty E(R,\Phi) R dR d\Phi + \int_0^{R_0} E(R,\Phi)[q(R)-1] R dR d\Phi,$$

where the exponential function in the integrand of Eq. (2) is denoted as E; hence, f becomes the sum of two integrals α and β multiplied by a common factor,

$$f(r) = \frac{i}{\lambda R_1 R_2} e^{-ik(R_1+R_2)} e^{-(ik/2R_1)\rho^2-(ik/2R_2)r^2} \left\{ \underbrace{\int_0^\infty R dR \int_0^{2\pi} e^{-ik/2(1/R_1+1/R_2)R^2+(ik/R_1)\rho R\cos(\theta-\Phi)+(ik/R_2)rR\cos\Phi} d\Phi}_{\alpha} \right.$$
$$\left. + \underbrace{\int_0^{R_0} R dR \int_0^{2\pi} [q(R)-1] e^{-ik/2(1/R_1+1/R_2)R^2+(ik/R_1)\rho R\cos(\theta-\Phi)+(ik/R_2)rR\cos\Phi} d\Phi}_{\beta} \right\}.$$

The term denoted α can be evaluated by noting that it is independent of Φ, permitting Φ to be taken as zero, completing the square in the argument of the exponential, and using the relation[12]

$$\int_0^{2\pi} e^{ia\sin(\zeta+\lambda)} d\zeta = 2\pi J_0(a),$$

which can also be shown to be independent of ζ, together with[13]

$$\int_0^\infty J_0(\beta x) e^{\pm iax^2} x dx = \pm \frac{i}{2a} e^{\mp i(\beta^2/4a)}$$

to give

$$\alpha = -\frac{2\pi i R_1 R_2}{k(R_1+R_2)} e^{[ikR_1R_2/2(R_1+R_2)][\rho^2/R_1^2+r^2/R_2^2+(2\rho r/R_1R_2)\cos\theta]}.$$

The second term denoted β can be reduced to

$$\beta = 2\pi \int_0^{R_0} [q(R) - 1] e^{-ik/2(1/R_1 + 1/R_2)R^2} J_0(kR\tilde{r}) R dR,$$

where the dimensionless quantity $\tilde{r}$ is defined as

$$\tilde{r} = \sqrt{\frac{\rho^2}{R_1^2} + \frac{r^2}{R_2^2} + \frac{2\rho r}{R_1 R_2} \cos\theta}.$$

III. IMAGE INTENSITY FOR A GAUSSIAN SOURCE

The intensity at the image plane for an incoherent source with a source intensity distribution $s(\rho)$ at the source plane is

$$I(r) = \int_0^{\infty} \int_0^{2\pi} s(\rho) |f(r)|^2 \rho d\rho d\theta.$$

For a Gaussian source with an intensity in the source plane described by $s(\rho) = (2\pi\sigma^2)^{-1} \exp(-\rho^2/2\sigma^2)$, where σ is the length parameter for the source, $I(r)$ becomes

$$I(r,\sigma) = \frac{1}{2\pi\sigma^2} \left[\frac{1}{(R_1 + R_2)} \right]^2 \int_0^{\infty} \int_0^{2\pi} \rho e^{-\rho^2/2\sigma^2} |\hat{\alpha} + \hat{\beta}|^2 d\rho d\theta, \tag{4}$$

where the dimensionless quantities $\hat{\alpha}$ and $\hat{\beta}$ are defined as

$$\hat{\alpha} = e^{[ikR_1R_2/2(R_1+R_2)][\rho^2/R_1^2 + r^2/R_2^2 + (2\rho r/R_1R_2)\cos\theta]}$$

and

$$\hat{\beta} = \frac{ik(R_1 + R_2)}{R_1 R_2} \int_0^{R_0} [q(R) - 1] e^{-ik/2(1/R_1 + 1/R_2)R^2} \times J_0(kR\tilde{r}) R dR.$$

Equation (4) can be written as the sum of three terms,

$$I(r,\sigma) = \frac{1}{2\pi\sigma^2} \left[\frac{1}{(R_1 + R_2)} \right]^2 [I_{\alpha\alpha^*} + 2\,\mathrm{Re}\, I_{\alpha\beta^*} + I_{\beta\beta^*}], \tag{5}$$

where

$$I_{\alpha\alpha^*} = \int_0^{\infty} \int_0^{2\pi} \rho e^{-\rho^2/2\sigma^2} d\rho d\theta = 2\pi\sigma^2,$$

$$I_{\alpha\beta^*} = \frac{-ik(R_1 + R_2)}{R_1 R_2} \int_0^{\infty} \int_0^{2\pi} e^{-\rho^2/2\sigma^2} e^{[ikR_1R_2/2(R_1+R_2)][\rho^2/R_1^2 + r^2/R_2^2 + (2\rho r/R_1R_2)\cos\theta]} \rho d\rho d\theta \int_0^{R_0} R[q(R) - 1]^* e^{ik/2(1/R_1 + 1/R_2)R^2} J_0(kR\tilde{r}) dR,$$

and

$$I_{\beta\beta^*} = \left[\frac{k(R_1 + R_2)}{R_1 R_2} \right]^2 \int_0^{\infty} \int_0^{2\pi} d\rho d\theta \rho e^{-\rho^2/2\sigma^2} \int_0^{R_0} [q(R) - 1] e^{-ik/2(1/R_1 + 1/R_2)R^2} J_0(kR\tilde{r}) R dR \times \int_0^{R_0} [q(R') - 1]^* e^{ik/2(1/R_1 + 1/R_2)R'^2} J_0(kR'\tilde{r}) R' dR'.$$

From the theory of Bessel functions[14] $J_0(kR\tilde{r})$ can be expanded as[15]

$$J_0(kR\tilde{r}) = \sum_m \varepsilon_m J_m\left(-kR\frac{\rho}{R_1}\right) J_m\left(kR\frac{r}{R_2}\right) \cos m\theta, \tag{6}$$

where ε_m is defined as $\varepsilon_m = 2$ for $m > 0$ and $\varepsilon_m = 1$ for $m = 0$. Through use of Eq. (6) and the orthogonality property of the cosine functions, $\int_0^{2\pi} \cos m\theta \cos n\theta d\theta = 2\pi$ if $m = n = 0$ and $\pi\delta_{m,n}$ otherwise, Eq. (5) becomes

$$I_{\alpha\beta^*} = \frac{(-i)^{m+1} 2\pi k(R_1 + R_2)\sigma^2}{\gamma R_1 R_2} e^{[ikR_1R_2/2(R_1+R_2)]r^2/R_2^2} \sum \varepsilon_m \int_0^{R_0} dR R[q(R) - 1]^* e^{ik/2(1/R_1 + 1/R_2)R^2} \times J_m\left(\frac{kr}{R_2}R\right) I_m\left(\frac{\sigma^2 k^2 rR}{\gamma R_1(R_1 + R_2)}\right) e^{-(k^2\sigma^2/2\gamma)[r^2/(R_1 + R_2)^2 + R^2/R_1^2]},$$

where I_m is a modified Bessel function and

$$I_{\beta\beta^*} = \left[\frac{k(R_1 + R_2)}{R_1 R_2} \right]^2 \pi\sigma^2 \sum g_m \varepsilon_m^2 \int_0^{R_0} dR R[q(R) - 1] e^{-ik/2(1/R_1 + 1/R_2)R^2} J_m\left(kR\frac{r}{R_2}\right) \times \int_0^{R_0} dR' R'[q(R') - 1]^* e^{ik/2(1/R_1 + 1/R_2)R'^2} J_m\left(kR'\frac{r}{R_2}\right) I_m\left(\frac{k^2\sigma^2 RR'}{R_1^2}\right) e^{-k^2\sigma^2(R^2 + R'^2)/2R_1^2}$$

where $g_m = 2$ for $m = 0$ and $g_m = 1$ for $m > 0$, and the parameter γ is given by

$$\gamma = 1 - i\frac{k(R_2/R_1)\sigma^2}{2(R_1+R_2)}.$$

Through straightforward algebraic manipulation, it is possible to write $I(r,\sigma)$ as a sum over dimensionless quantities as

$$I(r,\sigma) = \left(\frac{1}{R_1+R_2}\right)^2 \left[1 + 2\,\mathrm{Re}\sum_{m=0}^{\infty}(-i)^{m+1}\varepsilon_m \hat{I}^{(m)}_{\alpha\beta^*}(r) + \sum_{m=0}^{\infty} g_m \varepsilon_m^2 \hat{I}^{(m)}_{\beta\beta^*}(r)\right], \tag{7}$$

where

$$\hat{I}^{(m)}_{\alpha\beta^*}(r) = \frac{k(R_1+R_2)}{\gamma R_1 R_2} e^{ikR_1R_2r^2/2(R_1+R_2)R_2^2} \times \int_0^{R_0} [q(R)-1]^* e^{ik/2(1/R_1+1/R_2)R^2} \times J_m\left(\frac{kr}{R_2}R\right) I_m\left(\frac{\sigma^2k^2rR}{\gamma R_1(R_1+R_2)}\right) \times e^{-(k^2\sigma^2/2\gamma)[r^2/(R_1+R_2)^2+R^2/R_1^2]} R\,dR,$$

$$\hat{I}^{(m)}_{\beta\beta^*}(r) = \frac{1}{2}\left[\frac{k(R_1+R_2)}{R_1R_2}\right]^2 \int_0^{R_0} [q(R)-1] \times e^{-ik/2(1/R_1+1/R_2)R^2} J_m\left(kR\frac{r}{R_2}\right) R\,dR \int_0^{R_0} [q(R')-1]^* \times e^{ik/2(1/R_1+1/R_2)R'^2} J_m\left(kr\frac{R'}{R_2}\right) I_m\left(\frac{k^2\sigma^2RR'}{R_1^2}\right) \times e^{-k^2\sigma^2(R^2+R'^2)/2R_1^2} R'\,dR'.$$

IV. IMAGE INTENSITY FOR POINT AND PARALLEL BEAM SOURCES

In the limit where the source can be approximated as a point source, i.e., where $\sigma=0$, the arguments of I_m become zero so that $I_m=\delta_{m,0}$ and the sums in Eq. (7) reduce to a single term. The parameter γ also becomes unity; thus the intensity reduces to the relatively simple expressions

$$I(r,0) = \left(\frac{1}{R_1+R_2}\right)^2 \left|1 + \frac{ik(R_1+R_2)}{R_1R_2}\, e^{-[ik(R_1/R_2)/2(R_1+R_2)]r^2} \times \int_0^{R_0} [q(R)-1] e^{-[ik/2(R_1+R_2)/(R_1R_2)]R^2} J_0\left(kr\frac{R}{R_2}\right) R\,dR\right|^2. \tag{8}$$

If the source-to-object distance becomes large compared with the object-to-image distance, i.e. if $R_1 \gg R_2$, Eq. (7) reduces to

$$I(r,0) = \frac{1}{R_1^2}\left|1 + \frac{ik}{R_2} e^{-(ik/2R_2)r^2} \int_0^{R_0} [q(R)-1] \times e^{-(ik/2R_2)R^2} J_0\left(kr\frac{R}{R_2}\right) R\,dR\right|^2, \tag{9}$$

which could be derived directly from Eq. (2). It is noteworthy that both Eqs. (8) and (9) are integrals over one coordinate and require no summation.

V. EXPERIMENTS AND CALCULATED IMAGES

Plots for the expressions derived above were made by computing intensity versus radius and shown with the radial coordinate extending in two directions to give a simulation of the intensity profile over a center slice of an image. The intensity patterns determined from theory were calculated with MATHEMATICA using a large number of significant figures. All calculated plots were referred to the object plane. Figure 2 shows the results of calculations for polystyrene spheres irradiated by a point source of x-radiation for two different x-ray photon energies, 1.7 and 30 keV. The source-to-object and object-to-image planes used in all of the calculations were $R_1=0.2$ m and $R_2=2.4$ m, giving a magnification of 13. The oscillatory features at the perimeters of the spheres are seen to be of lower frequency and of smaller amplitude in the plot calculated with the lower energy x-radiation. Oscillatory features at the centers of the images are present in the plots at both x-ray energies, albeit with a significantly smaller amplitude at 30 keV.

A similar plot for a 100 μm diameter gold sphere calculated for a point source is shown in Fig. 3. Strong absorption contrast is seen in central region of the plot. Despite the strong absorption of gold at a photon energy of 1.7 keV, oscillations in the intensity near $r=0$ arising from interferences are still found.

Calculations for images of nylon and gold spheres for a nonvanishing x-radiation source are shown in Fig. 4. The phase contrast features are virtually all absent in the plot for the gold sphere but remain as easily visible features for the nylon sphere. Experiments were carried out using a microfocus x-ray tube (Oxford, Inc., Model UM-M1) with an anode source diameter, as specified by the manufacturer, of 13.5 μm together with a Peltier effect cooled charge coupled device (CCD) camera (Princeton Instruments, Model PI-SCX) equipped with a fiber optic bundle that views a phosphor plate to give an input-to-output image size ratio of unity. Further details of the experimental apparatus can be found in Ref. 8.

In order to determine the capability of the microfocus x-ray apparatus for imaging small spherical objects, experiments were carried out with polystyrene spheres of various diameters (purchased from Duke Scientific Co.) As shown in Fig. 5, experiments with several different diameter polystyrene and gold spheres indicate that the visualization of polystyrene spheres larger than 20 μm is facile owing to the distinctive dark and light outlines of the spheres provided by phase contrast; distinguishing polystyrene objects with features smaller than 10 μm from the background however is

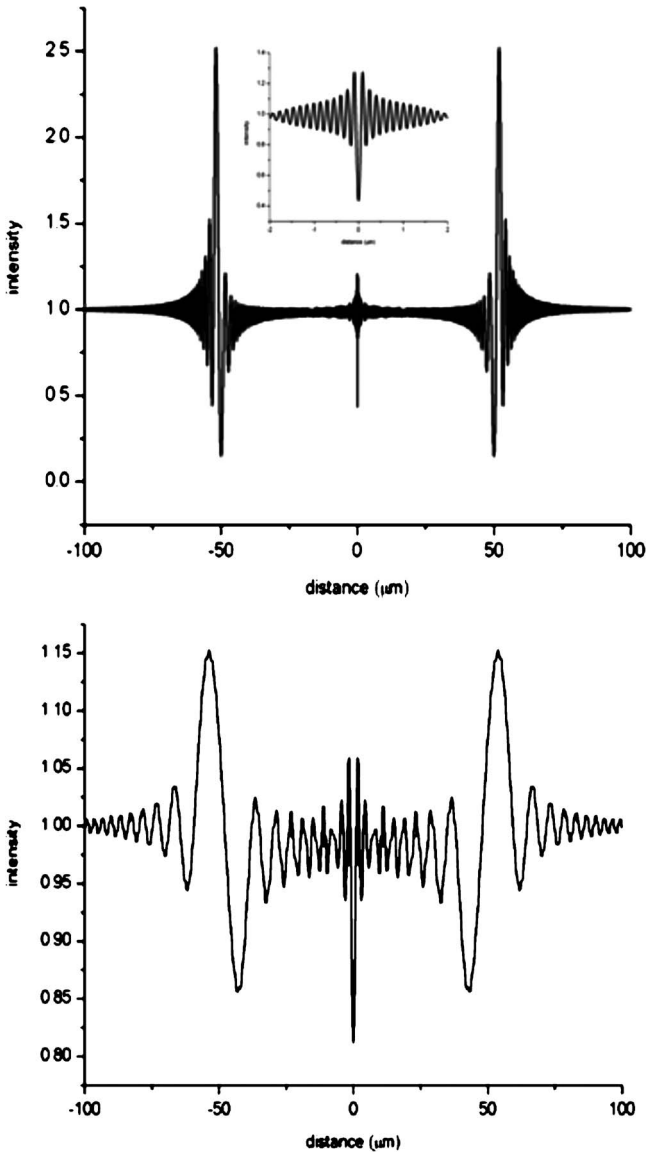

FIG. 2. Intensity vs radial coordinate calculated from Eq. (8) for a 100 μm diameter polystyrene sphere with $\delta=10^{-6}$ and $\mu_0=0$, irradiated by a point source of x-radiation. The x-ray photon energy is (top) 30 keV and (bottom) 1.7 keV, corresponding to wavelengths of 24 and 730 pm, respectively. Inset: expanded view of the center of the 30 keV plot.

difficult. The nearly spherical gold particles were made by scattering 325 mesh gold powder on a glass cover slide, and heating the glass with a torch until fusion of the metal was observed. This procedure produced approximately spherical particles with a random distribution of diameters. Although there is virtually no phase contrast seen in Fig. 5 for the gold spheres, the absorption contrast of gold is sufficiently large that particles larger than 10 μm could be seen easily against the background.

VI. DISCUSSION

A feature of the point source calculations given here that appears to be unique to objects with cylindrical symmetry is the appearance of intensity variations amounting to what would be a "bright spot" at image plane on the symmetry axis of the object, as shown in Figs. 2 and 3. The observation

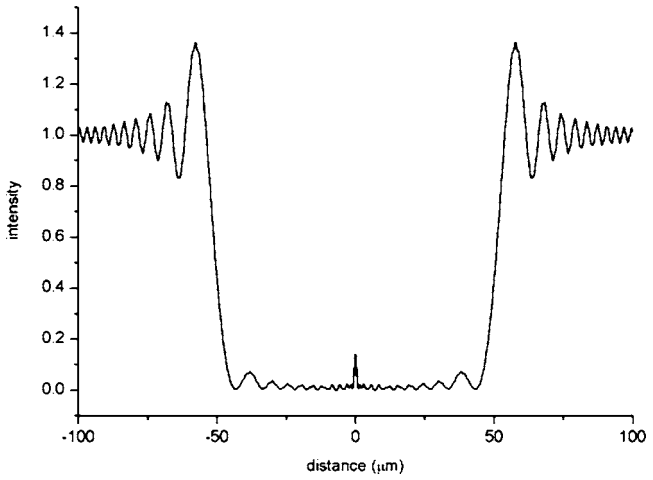

FIG. 3. Intensity in arbitrary units vs radial coordinate calculated from Eq. (8) for a 100 μm diameter gold sphere with $\delta=3.56\times10^{-6}$ and $\mu_0=2.5\times10^4$ m^{-1}, irradiated by a point source of x-radiation. The x-ray photon energy is 1.7 keV.

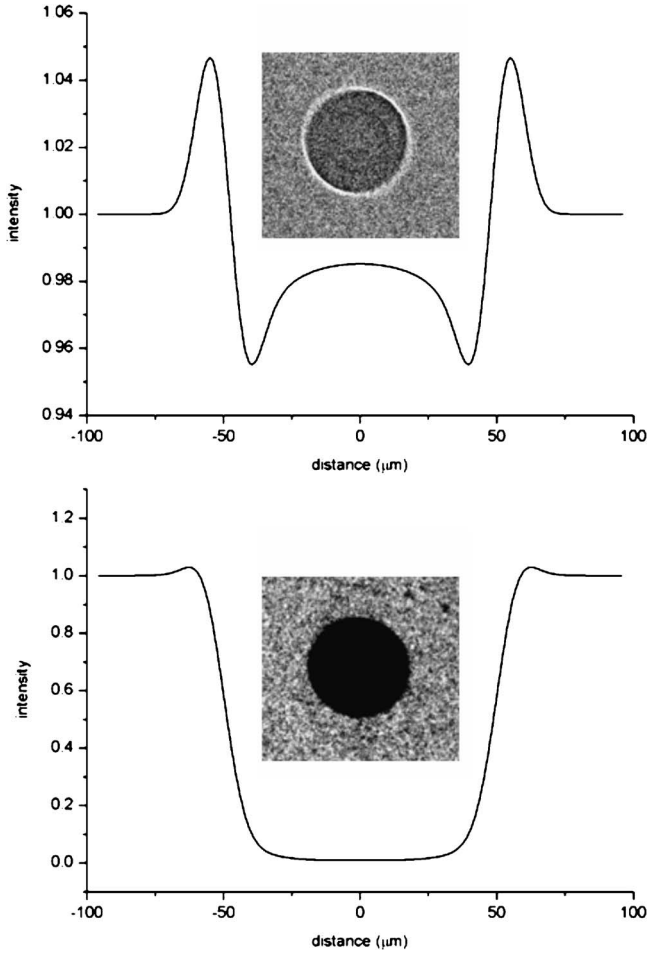

FIG. 4. Intensity vs radial coordinate calculated from Eq. (7) for (top plot) a 100 μm diameter sphere with $\delta=1\times10^{-6}$ and $\mu_0=0$ and (bottom plot) a 100 μm diameter gold sphere with $\delta=3.56\times10^{-6}$ and $\mu_0=2.5\times10^4$ m^{-1}, irradiated by an x-ray source with the source diameter parameter $\sigma=6.75$ μm and an x-ray photon energy of 1.7 keV. The insets are images of (top) a 100 μm diameter polystyrene sphere and (bottom) a 220 μm diameter gold sphere. Both images were taken with the x-ray tube operating for 3 min at 90 kV and 100 μA. The intensity patterns determined from theory were calculated with MATHEMATICA using a large number of significant figures.

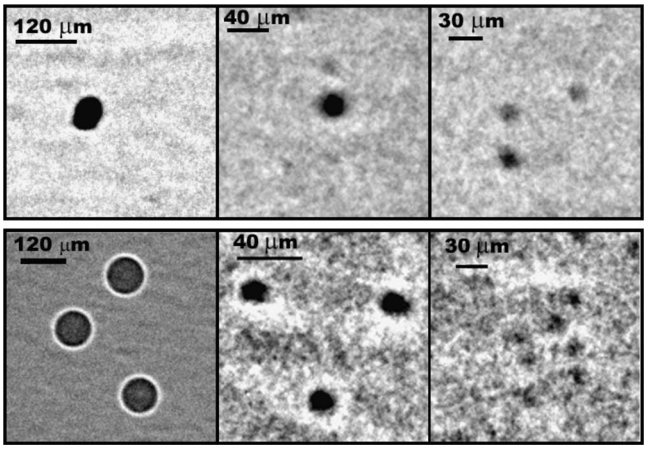

FIG. 5. X-ray images of (top) gold particles and (bottom) polystyrene spheres. The polystyrene spheres are nominally 100, 20, and 10 μm in diameter. The exposure time was 15 min with the x-ray tube operating at 90 kV and 100 μA.

of a bright spot radiation as a result of interposing an opaque circular disk between a visible light source and the image plane dates back almost 2 centuries to the time when Fresnel submitted his theory of imaging[9] to the French Academy; although the effect is counterintuitive, it is easily demonstrated in the laboratory with visible light and is a feature that is present over a range of wavelengths. As is shown here, the total number of photons in the central region diminishes greatly as the wavelength of the radiation is made short so that for radiation corresponding to an energy of 30 keV, there is little evidence of a bright spot.

The use of nanometer sized particles tagged with site directed antibodies to target specific tissues has become common practice in imaging and drug delivery and even holds promise for therapy. The high sensitivity of x-ray phase contrast imaging for detecting small objects may have similar application for locating particles such as polystyrene or gold in soft tissue. Although heavy metal objects such as gold particles do not produce phase contrast to the same degree that objects with smaller values of δ do under the conditions used in the experiments reported here, the high resolution of the method permits visualization of spheres with diameters of the order of 20 μm. The results of this study show that for the 20 μm x-ray source size, polystyrene and gold spheres with diameters of the order of the source size can be distinguished reliably from the background. Although a rigorous study has not been carried out, the present results suggest that x-ray sources with smaller source sizes should be capable of distinguishing even smaller particles from a low density background.

ACKNOWLEDGMENTS

Some of the authors (G.J.D., T.J.H., and G.C.) and G.J.D. and C.R.P. are grateful for the support of this research by the U.S. Army Medical Research and Materiel Command under Grant Nos. DAMD17-02-1-0307 and W81XWH-04-1-0481, respectively. C.R.P. acknowledges partial support from the U.S. Department of Energy under Grant No. DE-FG02-08ER15937. C.M.L. was supported by NIH under Grant No. T32 DK60415. Opinions, interpretations, conclusions, and recommendations are those of the authors and are not necessarily endorsed by the U.S. Army.

[1] P. Cloetens, R. Barrett, J. Baruchel, J.-P. Guigay, and M. Schlenker, J. Phys. D **29**, 133 (1996).
[2] S. W. Wilkins, T. Gureyev, D. Gao, A. Pogany, and A. W. Stevenson, Nature (London) **384**, 335 (1996).
[3] F. Arfelli, M. Assante, V. Bonvicini, A. Bravin, G. Cantatore, E. Castelli, L. D. Palma, M. DiMichiel, R. Longo, A. Olivo, S. Pani, D. Pontoni, P. Poropat, M. Prest, A. Rashevsky, G. Tromba, A. Vacchi, E. Vallazza, and F. Zanconati, Phys. Med. Biol. **43**, 2845 (1998).
[4] P. Cloetens, W. Ludwig, J. Baruchel, D. V. Dyck, J. V. Landuyt, J. P. Guigay, and M. Schlenker, Appl. Phys. Lett. **75**, 2912 (1999).
[5] S. Zabler, P. Cloetens, J. P. Guigay, J. Baruchel, and M. Schlenker, Rev. Sci. Instrum. **76**, 073705 (2005).
[6] C. J. Bailat, T. J. Hamilton, C. Rose-Petruck, and G. J. Diebold, Appl. Phys. Lett. **85**, 4517 (2004).
[7] T. J. Hamilton, C. J. Bailat, C. Rose-Petruck, and G. J. Diebold, Phys. Med. Biol. **49**, 4985 (2004).
[8] G. Cao, T. J. Hamilton, C. Rose-Petruck, and G. J. Diebold, J. Opt. Soc. Am. A Opt. Image Sci. Vis **24**, 1201 (2007).
[9] M. Born and E. Wolf, *Principles of Optics* (Pergamon, Oxford, 1980).
[10] J. M. Cowley, *Diffraction Physics* (North-Holland, Amsterdam, 1984).
[11] M. V. Klein, *Optics* (Wiley, New York, 1970).
[12] I. S. Gradshteyn and I. M. Ryzhik, *Table of Integrals, Series, and Products*, 4th ed. (Academic, New York, 1965).
[13] The first of these can be shown to be independent of λ and to yield the zeroth order Bessel function. The second is a combination of two integrals found in Ref. 12.
[14] G. N. Watson, *A Treatise On The Theory of Bessel Functions*, 2nd ed. (Cambridge University Press, Cambridge, 1996).
[15] The identity in the text follows from Neumann's addition theorem in Ref. 14.